Nuclear Materials and Energy 12 (2017) 283–288

Contents lists available at ScienceDirect

Nuclear Materials and Energy

journal homepage: www.elsevier.com/locate/nme

The role of rectified currents in far-field RF sheaths and in SOL losses of HHFW power on NSTX

R.J. Perkins*, J.C. Hosea, M.A. Jaworski, R.E. Bell, N. Bertelli, G.J. Kramer, L. Roquemore, G. Taylor, J.R. Wilson

Princeton Plasma Physics Laboratory, Princeton, New Jersey, USA

ARTICLE INFO

Article history:
Received 15 July 2016
Revised 18 April 2017
Accepted 22 April 2017
Available online 15 May 2017

ABSTRACT

Radio-frequency (RF) rectification is an important sheath phenomenon for wave heating of plasma in fusion devices and is proposed to be the mechanism responsible for converting high-harmonic fast-wave (HHFW) power in the National Spherical Torus eXperiment (NSTX) into a heat flux to the divertor. RF rectification has two aspects: current rectification and voltage rectification, and, while the latter is emphasized in many application, we demonstrate the importance of current rectification in analysis of the NSTX divertor during HHFW heating. When rectified currents are accounted for in first-principle models for the heat flux to the tiles, we predict a sizeable enhancement for the heat flux in the presence of an RF field: for one case studied, the predicted heat flux increases from 0.103 MW/m^2 to 0.209 MW/m^2. We also demonstrate how this rectification scales with injected HHFW power by tracking probe characteristics during a HHFW power ramp; the rectified current may be clamped at a certain level. This work is important for minimizing SOL losses of HHFW power in NSTX-U but may also have implications for near-field studies of ICRF antennae: ignoring rectified current may lead to underestimated heat fluxes and overestimated rectified voltages.

1. Introduction

Radio-frequency (RF) rectification refers to a sheath phenomena by which an RF potential across the sheath produces a time-averaged change in either sheath current, sheath voltage, or both. The RF fields tend to increase the average electron current flowing through the sheath; we refer to this effect as current rectification. The plasma potential *may* increase in order to offset, or screen, the enhanced electron current; we refer to this as voltage rectification. We propose three possible sheath responses to an RF voltage, illustrated in Fig. 1: (i) an increased electron current with no change in plasma potential, (ii) an increase in plasma potential to completely cancel the increased electron current, or (iii) partial screening, in which both rectified a electron current and plasma potential are present. While response (ii) is assumed on the basis of local ambipolarity in many applications of RF rectification, data from Langmuir probes embedded in the divertor of the National Spherical Torus eXperiment (NSTX) during high-harmonic fast-wave (HHFW) heating clearly show rectified currents, indicating either response (i) or (iii) but not (ii). For NSTX conditions, we will show that the calculated increase in heat flux to the divertor tiles due to RF rectification is greater for response (i) than (ii). Also, we follow the evolution of a probe characteristic during an HHFW power ramp, giving the degree of rectification as a function of RF voltage. The primary motivation for this work is to quantify the role of RF rectification in scrape-off layer (SOL) losses of HHFW power on NSTX, but there may be implications for the impact of RF rectification at ion-cyclotron range of frequencies (ICRF) antennas.

RF rectification plays a somewhat unconventional role in the NSTX divertor during HHFW heating. The HHFW system launches fast waves at frequencies well above the ion-cyclotron frequency electron heating and current drive [1], but experiments have shown a significant loss of HHFW power directly to the SOL [2]. During such experiments, bright and hot spirals form on the upper and lower divertor (Fig. 2); infrared (IR) cameras measure a heat flux within these spirals up to 2 MW/m^2 for an applied RF power of 1.8 MW [3], while up to 60% of the coupled HHFW power is estimated to be missing from the core plasma. In Ref. [4], we proposed that RF rectification is the mechanism responsible for converting wave power into a heat flux [4], with the RF sheaths

* Corresponding author.
E-mail address: rperkins@pppl.gov (R.J. Perkins).

http://dx.doi.org/10.1016/j.nme.2017.04.013

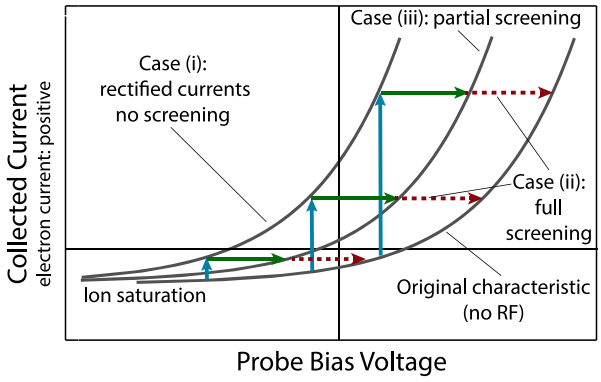

Fig. 1. Possible response of a Langmuir probe characteristic to RF rectification. The vertical blue arrows show the increase in collected electron current due to RF averaging, with no change in plasma potential. This changes the original characteristic (righthand exponential curve) to the leftmost curve (case (i)). The horizontal green arrows show the effect of increasing plasma potential to partially offset the increased electron current. For even an even greater increase in plasma potential (red dashed line), the increased electron current is completely screened (case (ii)). (For interpretation of the references to colour in this figure legend, the reader is referred to the web version of this article.)

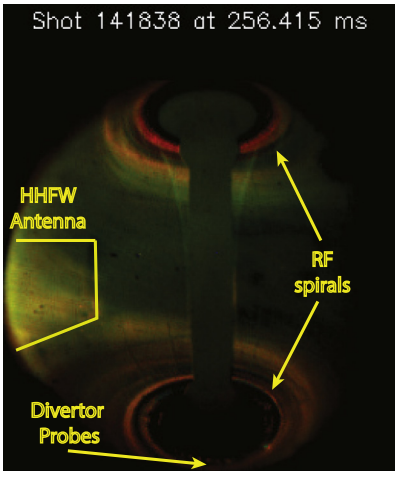

Fig. 2. Fast-camera image of NSTX during HHFW heating for shot 141838, an H-mode plasma with 1.2 MW of HHFW power and no neutral beam injection. Time of image is 256.4 ms with a background subtraction of eight frames starting at 215.2 ms. HHFW-antenna, HHFW-spiral, and divertor-probe positions are indicated.

being driven by enhanced wave fields due to cavity-like modes in the SOL [5,6]. This constitutes an instance of far-field sheaths [7], where propagating waves intercept a material surface some distance away from the antenna. However, unlike the more conventional picture in which far-field sheaths are established by wave power gradually leaving the core in regimes of low single-pass absorption [7,8], RF rectification in the NSTX divertor occurs prior to wave energy reaching the core, as NSTX has a high single-pass absorption rate for such waves [9]. It is of great importance for the HHFW program to determine the scaling of the heat flux driven by RF rectification as a function of the RF potential across the sheath.

RF rectification has a broad scope of applications in the fusion community beyond SOL losses of HHFW power.

1. RF rectification has been incriminated for the increased production of impurities that often accompany ICRH [10–12], as the rectified sheath voltage may accelerate ions to sufficient energies to enhance sputtering.
2. RF rectification threatens antenna components with premature demise due either to erosion of antenna components via ion bombardment and also overheating at hot spots, or regions of enhanced heat flux [13–15].
3. RF rectification has been hypothesized to explain modifications to the SOL during ICRF operation [16–18].
4. RF rectification presents a potential power sink for RF wave power [7] both for regimes of poor single-pass absorption and the NSTX case of prompt loss.

Much work on RF sheaths focuses on enhanced ion bombardment due to its potential for impurity production. Early consideration of the heat flux to the antenna due to RF rectification only incorporated the rectified-voltage (ion-bombardment) contribution [10], a paradigm that is still applied to heat loads at antennas [15,19–22] and to far-field sheaths [23]. The present work, focused on the role of rectified currents, may impact these other application of rectification in two ways: first, we calculate that incorporating rectified currents can greatly increase the heat flux due to rectification, and, second, for a measured V_{RF}, neglecting rectified currents will tend to overestimate the predicted change in rectified sheath voltage, potentially impacting sputtering studies.

We note that rectified currents due to ICRF operation have long been observed at or magnetically-connected to the active antennas in tokamaks [16,24,25] and are still observed on modern antennas [11]. Recent modeling has also begun to incorporate DC currents [26]. Moreover, SOL currents are known to exist without RF heating, originating from parallel or cross-field temperature gradients [27, chap. 17] or from drifts, and their effect on the heat flux to divertor tiles have been studied [28].

2. Ion and electron contributions to RF-driven sheath heat fluxes

This section develops the formulas for rectified currents and rectified voltages as introduced above. These formulas will also be used to separate the heat flux due to RF rectification into ion-bombardment and thermal-electron components. We will apply these formulas to probes embedded in divertor tiles, assuming that the probe and tile experience the same plasma conditions, and further that the probe bias does not alter the plasma potential of the flux tube linking the probe.

It is convenient to assume a Maxwellian electron distribution, which leads to the usual IV characteristic for a probe biased to voltage V relative to the vessel, for biases below the plasma potential:

$$I(V) = I_{\mathrm{sat}}\left(-1 + \frac{e^{(V-V_{fl}^{noRF})/T_e}}{1-\delta_e}\right). \tag{1}$$

I_{sat} is the ion saturation current. δ_e is the coefficient of secondary electron emission, which can be ignored for grazing incidence magnetic fields [29] (such as occurs in the divertor) but might be important for antenna components. V_{fl}^{noRF} is the floating potential without RF. The first term inside the parentheses is the ion current and is independent of V for bias below plasma potential; the second is the electron current. Voltages are defined relative to vessel potential. Therefore, the current collected by the divertor tile can be obtained simply by setting $V = 0$.

We consider two modifications to Eq. (1): the superposition of an RF voltage $V_{RF}\cos\omega t$ over the bias voltage V, and a change in plasma potential ΔV_{pl}. We do not, a priori, assume a relationship between these two quantities. We do assume, as mentioned above, the ΔV_{pl} is the same for both probe and tile. Considering at first only the RF voltage, the ion current is unaffected, and the electron current time-averages to:

$$\left\langle I^{-}(V)\right\rangle_{RF} = \frac{I_{\mathrm{sat}}}{1-\delta_e} I_0\left(\frac{V_{RF}}{T_e}\right) \exp\left(\frac{V-V_{fl}}{T_e}\right), \tag{2}$$

with I_0 the modified Bessel function [30]. The notation $\langle \ldots \rangle_{RF}$ will be used to denote quantities averaged over an RF cycle. To incoporate the change in plasma potential, we add ΔV_{pl} to the floating potential V_{fl}^{noRF}. This assumes that the common textbook relationship between plasma potential and floating potential [27],

$$V_{fl}^{noRF} = V_{pl} + \frac{1}{2}\ln\left[2\pi\frac{m_e}{m_i}\left(1+\frac{T_i}{T_e}(1+\delta_e)^{-2}\right)\right], \tag{3}$$

continues to hold in the presence of the RF fields. We plan to test this assumption in future HHFW experiments. Combining both modifications to Eq. (1) yields

$$\langle I(V)\rangle_{RF} = I_{\rm sat}\left(-1+I_0\left(\frac{V_{RF}}{T_e}\right)\frac{e^{(V-V_{fl}^{noRF}-\Delta V_{pl})/T_e}}{1-\delta_e}\right). \tag{4}$$

If we define

$$V_{fl}^{RF} = T_e \ln I_0\left(\frac{V_{RF}}{T_e}\right), \tag{5}$$

then Eq. (4) becomes

$$\langle I(V)\rangle_{RF} = I_{\rm sat}\left(-1+\frac{e^{(V+V_{fl}^{RF}-V_{fl}^{noRF}-\Delta V_{pl})/T_e}}{1-\delta_e}\right), \tag{6}$$

and the new floating potential is $V_{fl}^{noRF} + \Delta V_{pl} - V_{fl}^{RF}$.

We now consider the different cases proposed for the sheath response to the RF fields. Case (i) assumes no change in plasma potential, $\Delta V_{pl} = 0$, so the probe characteristic is effectively shifted negative by an amount V_{fl}^{RF} and, at any bias voltage V, the probe collects more electron current than without the RF. In case (ii), we assume $\Delta V_{pl} = V_{fl}^{RF}$. The means that, for bias V below $V_{pl} - V_{RF}$, the probe charactersitic is unaltered, and the probe collects the same current as it would without RF. Finally, case (iii) corresponds to an intermediate situation with $0 < \Delta V_{pl} < V_{fl}^{RF}$. Cases (i) and (ii) are complimentary, and we can make a circuit analogy in which RF rectification plays the role of a non-ideal voltage (or current) source. In case (i) the plasma-sheath system acts as though it has infinite impedance to ground, allowing no rectified current to flow in exchange for an elevated mean (rectified) voltage ((this is clearly akin to a floating condition). Case (ii) behaves as though there was zero impedance to ground and conducts the rectified current with no change in voltage.

The RF-averaged heat flux $< Q(V) >_{RF}$ to a surface biased at potential V is given by [4]

$$\langle Q(V)\rangle_{RF} = -I_{\rm sat}(V - V_{pl}^{noRF} + \Delta V_{pl}) + 2.5T_i I^{sat} + \ldots \frac{2}{1-\delta_e} I^{sat} T_e I_0\left(\frac{V_{RF}}{T_e}\right) e^{(V-V_{fl}^{noRF}-\Delta V_{pl})/T_e} \tag{7}$$

$$= -I_{\rm sat}V + 2.5T_i J^{sat} + \frac{2}{1-\delta_e} J_{RF}^{-} T_e, \tag{8}$$

Eq. (7) is straightforward extension of the no-RF case [27]. The first term of Eq. (7) is the energy gained by the ions as they fall through the sheath potential. Since this term is linear in V, the RF voltage simply averages out, but this term contributes when $\Delta V_{pl} \neq 0$. The second term is the energy flux (flow plus thermal) of the ions at the sheath edge, which is independent of V and is rather set by the Bohm sheath criteria. It does not get directly modified by the RF potential. The last term is the thermal energy flux from the electrons and is proportional to the rectified electron current, Eq. (2).

We would like to extract from Eq. (7) the portion of the heat flux due solely to rectification. Denoting this quantity ΔQ_{RF}, we find

$$\Delta Q_{RF} = \Delta V_{pl} I^{sat} + \ldots \frac{2I^{sat}T_e}{1-\delta_e} e^{(V-V_{fl}^{noRF})/T_e}\left(I_0\left(\frac{V_{RF}}{T_e}\right)e^{-\Delta V_{pl}/T_e} - 1\right). \tag{9}$$

The thermal heat flux from the ions drops out from Eq. (9). Clearly, the larger ΔV_{pl}, the greater the ion bombardment term but the smaller the electron thermal contribution. In the case of perfect screening (case (ii)), the electron term of Eq. (7) tends to zero:

$$\Delta Q_{RF,rv} = \Delta V_{pl} I_{\rm sat} = T_e I_{\rm sat} \ln\left(I_0\left(\frac{V_{RF}}{T_e}\right)\right) \tag{10}$$

with the subscript "rv" denoting "rectified voltage." This equation is frequently used in the ICRF community [15,19–21] for the heat flux due to RF rectification and assumes that ion bombardment dominates, even for far-field sheath dissipation [23]. The validity of this assumption will be discussed in Section 4. In the case of no screening, $\Delta V_{pl} = 0$, so

$$\Delta Q_{RF,rc} = \frac{2I_{\rm sat}T_e}{1-\delta_e} e^{(V-V_{fl}^{noRF})/T_e}\left(I_0\left(\frac{V_{RF}}{T_e}\right) - 1\right), \tag{11}$$

with the subscript "rc" denoting rectified currents. In the limit $V_{RF} \gg T_e$, Eq. (11) scales nearly exponentially with V_{RF}, indicating that, at some point, the plasma must begin to screen the rectified currents, and the heat flux scaling will transition over to Eq. (10).

It is natural to inquire which response above gives the greater heat flux for a given V_{RF}/T_e. However, direct comparison of Eqs. (11) and (10) requires knowing the additional parameter in Eq. (11): $(V - V_{fl}^{noRF})/T_e$. In general, for $V_{RF} \gg T_e$, Eq. (11) yields a ΔQ much greater than Eq. (10), as Eq. (11) asymptotes to $\exp(V_{RF}/T_e)/(V_{RF}/T_e)^{1/2}$ while Eq. (10) asymptotes to V_{RF}/T_e. Analyzing the opposite, limit, we find that if

$$\frac{2}{1-\delta_e}\exp\frac{V - V_{fl}^{noRF}}{T_e} > 1, \tag{12}$$

Eq. (11) produces a greater ΔQ_{RF} than Eq. (10) for all V_{RF}. However, if Eq. (12) does not hold, then there is some value of V_{RF}/T_e below which Eq. (10) exceeds Eq. (11). That being said, we find that, for NSTX divertor tiles (presented in Section 3), Eq. (12) is usually well satisfied so that Eq. (11) always produces the larger heat flux. We note that Eqs. (11) and (10) represent extreme cases as discussed above, and the actual ΔQ_{RF} should fall somewhere inbetween.

3. Application to SOL losses in the NSTX divertor

Section 2 laid the groundwork for how three key sheath quantities: current, voltage, and heat flux, are rectified. In the NSTX divertor, swept Langmuir probe data indicate that the divertor tiles draw a rectified electron current during HHFW heating. This response rules out the possibility of perfect screening by increased plasma potential, although the possibility of partial screening is discussed in Section 4. In this section, we present analysis results assuming case (i), no change in plasma potential. To highlight the important role of the rectified current, we also present analysis assuming perfect screening. In all NSTX cases studied, we find that assuming rectified current produces a larger heat flux than assuming rectified voltages.

Table 1 summarizes the present analysis for three cases studied in Ref. [4]. In each case, the RF spiral fell over a radial array of swept Langmuir probe embedded in lower-divertor tiles, and a negative shift in floating potential was observed with little change in electron temperature for a probe that was located underneath the RF spiral compared to a nearby probe that was not underneath the spiral. The first five columns reflect information about the discharge and the probe characteristic, all of which are independent of the model used for RF rectification. $V_{fl,ob}$ is the *observed* floating potential with RF. We express heat flux in terms of the dimensionless heat transmission factor γ defined as $Q = I_{\rm sat}T_e\gamma$, and $\gamma_{\rm noRF}$ is the transmission factor in the absence of HHFW heating. The next two columns reflect calculations done assuming case (i): that there is no change in plasma potential. As discussed below in

Table 1
Analysis of Langmuir probe data from different NSTX discharges. P_{RF} is the amount of HHFW power applied, T_e is the electron temperature determined from fitting the probe characteristic, V_{fl}^{noRF} is the floating potential without HHFW heating, $V_{fl,ob}$ is the observed floating potential with HHFW, and γ_{noRF} is the sheath heat transmission factor without RF. $\Delta\gamma_{RF}$ is the change in γ due to rectification for both assumptions of rectified currents and rectified voltages.

Discharge data		Probe data				Case (i)		Case (ii)	
Shot	P_{RF} [MW]	T_e [eV]	V_{fl}^{noRF} [V]	$V_{fl,ob}$ [V]	γ_{noRF}	V_{RF} [V]	$\Delta\gamma_{RF,rc}$	ΔV_{pl} [V]	$\Delta\gamma_{RF,rv}$
141,899	1.5	13.5	4	−20	7.4	44	7.3	24	1.8
141,836	1.1	30	5	−23	6.5	64	2.5	28	0.92
141,830	0.55	22.5	1	−10	6.6	33	1.2	11	0.49

Section 4, this is the most conservative assumption. We calculate V_{RF} using Eq. (5). From this we then calculate $\Delta\gamma_{RF,rc}$, the change in γ due to RF rectification assuming rectified currents. The final two columns indicate results that would be been obtained assuming perfect screening (case (ii)) using the same V_{RF} value. The table shows the hypothetical change in plasma potential and also $\Delta\gamma_{RF,rv}$, which is substantially smaller than for rectified currents.

We now analyze characteristics from a single probe (Probe 1, major radius 63.82 cm, see Fig. 2) during the 10 ms HHFW power ramp. The sweep rate is 1 kHz, so this ramp presents the opportunity to observe the probe characteristic evolution with increasing RF voltage. The individual IV characteristics have large fluctuations, presumably from SOL/divertor turbulence [31,32], so that the uncertainty in the fit parameters obscures the effects of RF rectification. To obtain more viable fits, we average each sweep with its two neighboring sweeps. This is a necessary compromise between time resolution and accuracy of the fitting procedure. We compute the standard deviation of collected current at each bias voltage for each average for use in the fitting procedure so that points with large variance are weighted less. Unfortunately, with the small sample size for each average, this procedure tends to produces a few points with exceptionally low variance, so that the χ^2-minimization routine is dominated by fitting to this handful of points. We thus set a minimum variance of 2.5 mA, which avoids this issue while still giving less weights to those points with large variance. Finally, it is known that, even without RF, including bias voltages well above the floating potential tends to skew the fit to higher temperatures [33]. The HHFW heating primarily lowers the probe floating potential, bringing more of the high-bias region into the sweep range. Also, an RF voltage causes the probe, at any bias V, to average from $V - V_{RF}$ to $V + V_{RF}$; potentially distorting the high-bias region if it samples voltages exceeding the plasma potential [30] or even regions of suppressed electron collection [4]. Finally, the high-bias region is most susceptible to error from averaging consecutive sweeps when V_{fl} is changing in time. For these reasons, we only include bias voltages less than $V_{fl} + 25$ V in each fit. An exponential curve of the form in Eq. (1) is then fit to the averaged characteristic using standard χ^2-minimization routines. The averaged characteristics over the full sweep range and accompanying fits over the restricted range are shown for four time slices in Fig. 3 for shot 141838, an H-mode discharge with 1.1 MW of HHFW power and no neutral beam injection.

Fig. 4 plots the fitted parameters against $< P_{RF} >$, the average RF power during the interval of averaging. Comparing Fig. 4a to b, the HHFW power primarily lowers V_{fl} with less pronounced and systematic effects on T_e and I_{sat}, consistent with conclusions drawn in Ref. [4]. This favors the hypothesis of a cavity-like mode driving the SOL losses of HHFW over the alternative hypothesis of parasitic plasma heating in front of the antenna. Fig. 4 plots the fitted floating potential against the mean RF power; V_{fl} falls relatively sharply with HHFW power but then appears to be clamped around −10 V. We speculate that the plasma begins to screen the rectified currents, preventing V_{fl} from dropping any more. However, changes in discharge conditions and evolution of the magnetic equilibrium, shifting the spiral location, can contribute as well. For this discharge, the 1.1 MW of applied HHFW power is more than a significant perturbation to the target plasma. Fig. 4c shows the computed value of V_{RF} obtained by inverting Eq. (5) and assuming that $\Delta V_{pl} = 0$. V_{RF} initially rises with $< P_{RF} >$ and then levels off. This is unusual, as we expect that V_{RF} is proportional to the antenna voltage, which scales as $P_{RF}^{1/2}$. When we fit a square-root function to the first four data points of Fig. 4c, the data quickly deviates from this trend at larger powers. We hypothesize that our working assumption of $\Delta V_{pl} = 0$ becomes invalid, causing an underestimation of V_{RF}. In Fig. 4d, we compute ΔQ_{RF} based on both Eqs. (11) and(10). As in Table 1, the assumption of no-screening always yields a larger heat flux via current rectification.

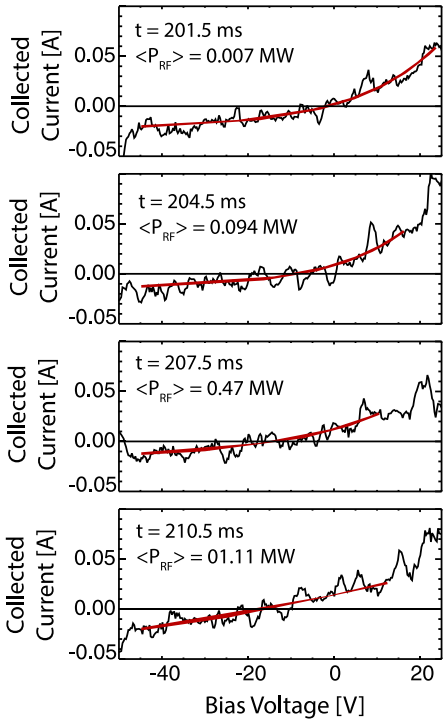

Fig. 3. Averaged probe characteristics taken during the 10 ms ramp HHFW. Despite averaging, sizable fluctuations are still visible. However, a clear downward shift in floating potential is seen as the HHFW power increases.

4. Discussion

In Section 3, we mentioned the possibility of partial screening: the change in floating potential observed on the probe, $\Delta V_{fl,ob}$, is a combined negative shift due to RF averaging of the collected cur-

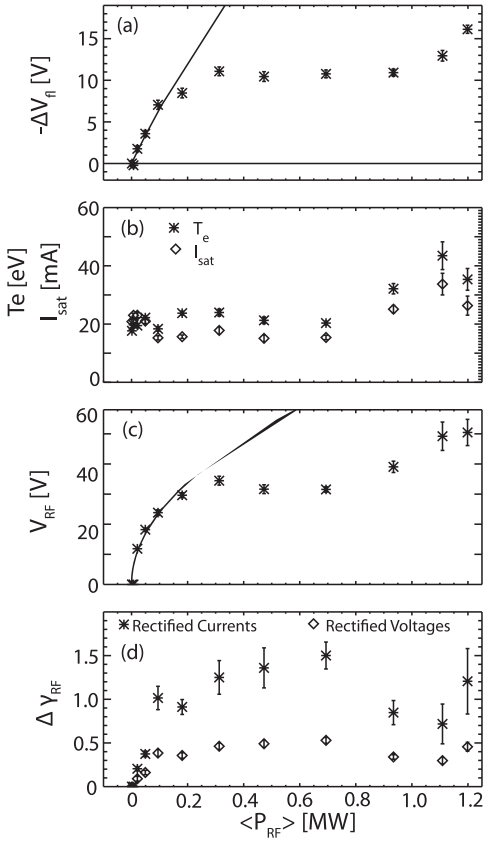

Fig. 4. Fit results from averaged IV characteristics during the HHFW ramp, plotted as a function of the average HHFW power during the averaging window. (a) Negative of the floating potential, (b) electron temperature and ion saturation current, (c) V_{RF}, assuming no change in plasma potential, and (d) ΔQ_{RF} expressed as the sheath heat transmission factor $\Delta\gamma_{RF} = \Delta Q_{RF}/T_e I_{sat}$, calculated both for the assumption of zero screening and full screening.

rent plus a positive change in plasma potential:

$$\Delta V_{fl,ob} = V_{fl}^{noRF} - V_{fl}^{RF} + \Delta V_{pl}, \tag{13}$$

with V_{fl}^{RF} a function of V_{RF} via Eq. (5). $\Delta V_{fl,\,ob}$ is given from the probe characteristic, but both ΔV_{pl} and V_{RF} are unknown. We can solve for V_{RF} as a function of ΔV_{pl}; in this case taking $\Delta V_{pl} = 0$, as done in Section 3, gives the smallest V_{RF} and also the smallest ΔQ_{RF} that is consistent with the observed change in floating potential. To prove the latter claim, note that, in Eq. (9), the thermal electron contribution is independent of ΔV_{pl} because it is proportional to the electron current, which is measured and fixed. The ion bombardment contribution, which is proportional to ΔV_{pl}, is obviously minimized when $\Delta V_{pl} = 0$. As noted in Ref. [4], our best extrapolation of heat flux to the probe location is larger than what is predicted with the probe sheath theory, which is consistent partial screening, but this is conjecture at this point. Note that the arguments of this paragraph use different constraints than those in the last paragraph of Section 2. Here, we are working with the constraint of a fixed probe floating potential given by probe measurements, whereas in Section 3 we fixed V_{RF}.

The NSTX swept probes do not, for practical reasons, sweep high enough to probe the plasma potential, so obtaining ΔV_{pl} may require dedicated techniques, such as emissive probes [34]. In principle, a floating non-emissive probe could measure changes in plasma potential, although this assumes that the textbook relationship between floating potential and plasma potential, Eq. (3)), continues to hold throughout the RF cycle. Note that the floating-probe method does not provide any information of the current drawn by the surrounding tile. An alternate approach that will be pursued on NSTX-U is to directly measure the RF component of the swept Langmuir probe signal to compute V_{RF} while retaining the DC measurements.

The rectified sheath currents described here are driven directly by the RF fields as opposed to indirectly via a thermoelectric effects. We conclude this based on the relatively large change in probe floating potential compared the smaller change in electron temperature seen in Fig. 4. It is natural to ask where these currents close. In early observations of ICRF-driven SOL currents, the currents were driven by sheaths at the active antenna and flowed along field lines to other strucutures, connecting through the vessel wall/liner [25]. In the present case, RF fields driving rectification are found in the divertor, due, as we hypothesize, to cavity-like modes in the SOL, and these divertor probes have long magnetic-connection lengths to the inner wall. We expect cross-field effects to play a more significant role in this case. We have also hypothesized that the current path may close through the vessel to the private flux region [35, P5.049].

While rectified currents are important in the analysis of the NSTX divertor, their impact at an ICRF antenna is less clear. We anticipate a greater degree of current screening at the antenna because V_{RF} should be much larger there since the rectified current, Eq. (2), scales nearly exponentially for $V_{RF} \gg T_e$. This would lead to very large (unrealistic) currents that, at some point, must be screened. Also, certain antenna components such as the Faraday screen bars are magnetically connected to other nearby components and act as a double probe system that could limit rectified currents [36]. That being said, rectified current to and from ICRF antennas have been observed [11,24,25]. The outer portions of the antenna limiter, for instance, have long magnetic connection lengths, so that cross-field diffusion can play a more important role and the rectified current may not be limited by the double-probe argument. Moreover, secondary electron emission may exacerbate the effect of rectified currents, as the angle of incidence on the limiter may not be low enough to suppress the secondaries. As argued in Sections 2 and 3, for a given V_{RF} the presence of rectified currents impacts calculations of both the heat flux to surfaces and the rectified voltage; assuming full screening would underestimate the heat flux and overestimate ion bombardment.

5. Conclusions

An RF potential across a sheath will drive a rectified current, a rectified voltage, or both, and the heat flux due to rectification is predicted to scale in different fashions for each case. In the divertor of NSTX during HHFW heating, rectified currents grow and then appear to saturate with increasing HHFW power. The predicted heat fluxes are substantially larger with the rectified current than those assuming rectified voltages. It is possible that similar conclusions may be reached for certain components of an ICRF antenna itself. This investigation will be continued on NSTX-U with dedicated divertor Langmuir probes equipped with electronics to measure the RF component of the signal, and also with midplane probes at the antenna. Also, IR thermography will be available for these probes, allowing validation of the scaling of heat flux with rectification.

Acknowledgment

This work was supported by DOE Contract No. DE-AC02-09CH11466. The digital data for this paper can be found at http://arks.princeton.edu/ark:/88435/dsp019306t1809.

References

[1] M. Ono, High harmonic fast waves in high beta plasmas, Phys. Plasmas 2 (11) (1995) 4075–4082. http://dx.doi.org/10.1063/1.871030.

[2] J. Hosea, R.E. Bell, B.P. LeBlanc, C.K. Phillips, G. Taylor, E. Valeo, J.R. Wilson, E.F. Jaeger, P.M. Ryan, J. Wilgen, H. Yuh, F. Levinton, S. Sabbagh, K. Tritz, J. Parker, P.T. Bonoli, R. Harvey, the NSTX Team, High harmonic fast wave heating efficiency enhancement and current drive at longer wavelength on the National Spherical Torus eXperiment, Phys. Plasmas 15 (5) (2008) 056104. http://dx.doi.org/10.1063/1.2837051.

[3] J.C. Hosea, R.E. Bell, E. Feibush, R.W. Harvey, E.F. Jaeger, B.P. LeBlanc, R. Maingi, C.K. Phillips, L. Roquemore, P.M. Ryan, G. Taylor, K. Tritz, E.J. Valeo, J. Wilgen, J.R. Wilson, the NSTX Team, Recent fast wave coupling and heating studies on NSTX, with possible implications for ITER, AIP Conf. Proc. 1187 (1) (2009) 105–112. http://dx.doi.org/10.1063/1.3273706.

[4] R.J. Perkins, J.C. Hosea, M.A. Jaworski, J.-W. Ahn, A. Diallo, R.E. Bell, N. Bertelli, S. Gerhardt, T.K. Gray, G.J. Kramer, B.P. LeBlanc, A. McLean, C.K. Phillips, M. Podestà, L. Roquemore, S. Sabbagh, G. Taylor, J.R. Wilson, The contribution of radio-frequency rectification to field-aligned losses of high-harmonic fast wave power to the divertor in the National Spherical Torus eXperiment, Phys. Plasmas 22 (4) (2015). http://dx.doi.org/10.1063/1.4916034.

[5] N. Bertelli, E. Jaeger, J. Hosea, C. Phillips, L. Berry, S. Gerhardt, D. Green, B. LeBlanc, R. Perkins, P. Ryan, G. Taylor, E. Valeo, J. Wilson, Full wave simulations of fast wave heating losses in the scrape-off layer of NSTX and NSTX-U, Nucl. Fus. 54 (8) (2014) 083004.

[6] N. Bertelli, E. Jaeger, J. Hosea, C. Phillips, L. Berry, P. Bonoli, S. Gerhardt, D. Green, B. LeBlanc, R. Perkins, C. Qin, R. Pinsker, R. Prater, P. Ryan, G. Taylor, E. Valeo, J. Wilson, J. Wright, X. Zhang, Full wave simulations of fast wave efficiency and power losses in the scrape-off layer of tokamak plasmas in mid/high harmonic and minority heating regimes, Nucl. Fus. 56 (1) (2016) 016019.

[7] J.R. Myra, D.A. D'Ippolito, M. Bures, Far field sheaths from waves in the ion cyclotron range of frequencies, Phys. Plasmas 1 (9) (1994) 2890–2900. http://dx.doi.org/10.1063/1.870529.

[8] C. Petty, F. Baity, J. deGrassie, C. Forest, T. Luce, T. Mau, M. Murakami, R. Pinsker, P. Politzer, M. Porkolab, R. Prater, Fast wave current drive in H mode plasmas on the DIII-D tokamak, Nucl. Fus. 39 (10) (1999) 1421.

[9] C. Phillips, R. Bell, L. Berry, P. Bonoli, R. Harvey, J. Hosea, E. Jaeger, B. LeBlanc, P. Ryan, G. Taylor, E. Valeo, J. Wilgen, J. Wilson, J. Wright, H. Yuh, the NSTX Team, Spectral effects on fast wave core heating and current drive, Nucl. Fus. 49 (7) (2009) 075015.

[10] M. Bures, J. Jacquinot, M. Stamp, D. Summers, D. Start, T. Wade, D. D'Ippolito, J. Myra, Assessment of beryllium faraday screens on the JET ICRF antennas, Nucl. Fus. 32 (7) (1992) 1139.

[11] Vl.V. Bobkov, F. Braun, R. Dux, A. Herrmann, L. Giannone, A. Kallenbach, A. Krivska, H. Müller, R. Neu, J.-M. Noterdaeme, T. Pütterich, V. Rohde, J. Schweinzer, A. Sips, I. Zammuto, the ASDEX Upgrade Team, Assessment of compatibility of ICRF antenna operation with full W wall in ASDEX upgrade, Nucl. Fus. 50 (3) (2010) 035004.

[12] A.N. James, D. Brunner, B. Labombard, C. Lau, B. Lipschultz, D. Miller, M.L. Reinke, J.L. Terry, C. Theiler, G.M. Wallace, D.G. Whyte, S. Wukitch, V. Soukhanovskii, Imaging of molybdenum erosion and thermography at visible wavelengths in alcator C-mod ICRH and LHCD discharges, Plasma Phys. Control. Fus. 55 (12) (2013) 125010.

[13] L. Colas, L. Costanzo, C. Desgranges, S. Brémond, J. Bucalossi, G. Agarici, V. Basiuk, B. Beaumont, A. Bècoulet, F. Nguyen, Hot spot phenomena on Tore Supra ICRF antennas investigated by optical diagnostics, Nucl. Fus. 43 (1) (2003) 1.

[14] K. Saito, T. Mutoh, R. Kumazawa, T. Seki, Y. Nakamura, N. Ashikawa, K. Sato, M. Shoji, S. Masuzaki, T. Watari, H. Ogawa, H. Takeuchi, H. Kasahara, F. Shimpo, G. Nomura, M. Yokota, C. Takahashi, A. Komori, Y. Zhao, J. Yoon, J. Kwak, ICRF Long-pulse discharge and interaction with a chamber wall and antennas in LHD, J. Nucl. Mater. 363–365 (2007) 1323–1328. Proceedings of the 17th International Conference on Plasma-Surface Interactions in Controlled Fusion Device. http://dx.doi.org/10.1016/j.jnucmat.2007.01.269.

[15] P. Jacquet, L. Colas, M.-L. Mayoral, G. Arnoux, V. Bobkov, M. Brix, P. Coad, A. Czarnecka, D. Dodt, F. Durodie, A. Ekedahl, D. Frigione, M. Fursdon, E. Gauthier, M. Goniche, M. Graham, E. Joffrin, A. Korotkov, E. Lerche, J. Mailloux, I. Monakhov, C. Noble, J. Ongena, V. Petrzilka, C. Portafaix, F. Rimini, A. Sirinelli, V. Riccardo, Z. Vizvary, A. Widdowson, K.-D. Zastrow, JET-EFDA Contributors, Heat loads on JET plasma facing components from ICRF and LH wave absorption in the SOL, Nucl. Fus. 51 (10) (2011) 103018.

[16] G.V. Oost, R.V. Nieuwenhove, R. Koch, A. Messiaen, P. Vandenplas, R. Weynants, K. Dippel, K. Finken, Y. Lie, A. Pospieszczyk, U. Samm, B. Schweer, R. Conn, W. Corbett, D. Goebel, R. Moyer, Invited paper: ICRF/edge physics research on TEXTOR, Fus. Eng. Des. 12 (1) (1990) 149–170. http://dx.doi.org/10.1016/0920-3796(90)90075-H.

[17] J.M. Noterdaeme, G.V. Oost, The interaction between waves in the ion cyclotron range of frequencies and the plasma boundary, Plasma Phys. Control. Fus. 35 (11) (1993) 1481.

[18] M. Bècoulet, L. Colas, S. Pécoul, J. Gunn, P. Ghendrih, A. Bècoulet, S. Heuraux, Edge plasma density convection during ion cyclotron resonance heating on Tore Supra, Phys.Plasmas 9 (6) (2002) 2619–2632. http://dx.doi.org/10.1063/1.1472501.

[19] L. Colas, P. Jacquet, G. Agarici, C. Portafaix, M. Goniche, JET-EFDA contributors, RF-Sheath heat flux estimates on Tore Supra and JET ICRF antennae. extrapolation to ITER, AIP Conf. Proc. 1187 (1) (2009a) 133–136. http://dx.doi.org/10.1063/1.3273711.

[20] L. Colas, D. Milanesio, E. Faudot, M. Goniche, A. Loarte, Estimated RF sheath power fluxes on ITER plasma facing components, J. Nucl. Mater. 390–391 (2009b) 959–962. Proceedings of the 18th International Conference on Plasma-Surface Interactions in Controlled Fusion Devices. http://dx.doi.org/10.1016/j.jnucmat.2009.01.248.

[21] P. Jacquet, F. Marcotte, L. Colas, G. Arnoux, V. Bobkov, Y. Corre, S. Devaux, J.-L. Gardarein, E. Gauthier, M. Graham, E. Lerche, M.-L. Mayoral, I. Monakhov, F. Rimini, A. Sirinelli, D.V. Eester, Characterisation of local ICRF heat loads on the JET ILW, J. Nucl. Mater. 438, Supplement (2013) S379–S383. Proceedings of the 20th International Conference on Plasma-Surface Interactions in Controlled Fusion Devices. http://dx.doi.org/10.1016/j.jnucmat.2013.01.075.

[22] D.A. D'Ippolito, J.R. Myra, Low-power fast wave antenna loading as a radio frequency sheath diagnostic, Phys. Plasmas 3 (1) (1996) 420–426. http://dx.doi.org/10.1063/1.871813.

[23] D.A. D'Ippolito, J.R. Myra, A radio-frequency sheath boundary condition and its effect on slow wave propagation, Phys. Plasmas 13 (10) (2006) 102508.

[24] R.V. Nieuwenhove, G.V. Oost, Experimental evidence for sheath effects at the ICRF antenna and ensuing changes in the plasma boundary during ICRF on TEXTOR, J. Nucl. Mater. 162 (1989) 288–291. http://dx.doi.org/10.1016/0022-3115(89)90284-5.

[25] R.V. Nieuwenhove, G.V. Oost, Experimental study of sheath currents in the scrape-off layer during ICRH on TEXTOR, Plasma Phys. Control. Fus. 34 (4) (1992) 525.

[26] L. Colas, J. Jacquot, S. Heuraux, E. Faudot, K. Crombé, V. Kyrytsya, J. Hillairet, M. Goniche, Self consistent radio-frequency wave propagation and peripheral direct current plasma biasing: simplified three dimensional non-linear treatment in the wide sheath asymptotic regime, Phys. Plasmas 19 (9) (2012). http://dx.doi.org/10.1063/1.4750046.

[27] P.C. Stangeby, The Plasma Boundary of Magnetic Fusion Devices, Plasma Physics Series (Taylor and Francis Group), 2000.

[28] D. Donovan, D. Buchenauer, J. Watkins, A. Leonard, C. Wong, M. Schaffer, D. Rudakov, C. Lasnier, P. Stangeby, Experimental measurements of the particle flux and sheath power transmission factor profiles in the divertor of DIII-d, J. Nucl. Mater. 438, Supplement (2013) S467–S471. Proceedings of the 20th International Conference on Plasma-Surface Interactions in Controlled Fusion Devices. http://dx.doi.org/10.1016/j.jnucmat.2013.01.095.

[29] S. Mizoshita, K. Shiraishi, N. Ohno, S. Takamura, Plasma-surface interactions in controlled fusion devices secondary electron emission from solid surface in an oblique magnetic field, J. Nucl. Mater. 220 (1995) 488–492. http://dx.doi.org/10.1016/0022-3115(94)00509-5.

[30] A. Boschi, F. Magistrelli, Effect of a r.f. signal on the characteristic of a langmuir probe, Il Nuovo Cimento 29 (2) (1963) 487–499, doi:10.1007/BF02750367.

[31] J.A. Boedo, J.R. Myra, S. Zweben, R. Maingi, R.J. Maqueda, V.A. Soukhanovskii, J.W. Ahn, J. Canik, N. Crocker, D.A. D'Ippolito, R. Bell, H. Kugel, B. Leblanc, L.A. Roquemore, D.L. Rudakov, the NSTX Team, Edge transport studies in the edge and scrape-off layer of the National Spherical Torus eXperiment with langmuir probes, Phys. Plasmas 21 (4) (2014) 042309. http://dx.doi.org/10.1063/1.4873390.

[32] S.J. Zweben, J.R. Myra, W.M. Davis, D.A. D'Ippolito, T.K. Gray, S.M. Kaye, B.P. LeBlanc, R.J. Maqueda, D.A. Russell, D.P. Stotler, the NSTX-U Team, Blob structure and motion in the edge of NSTX, Plasma Phys. Control. Fus. 58 (2016) 044007.

[33] J.A. Tagle, P.C. Stangeby, S.K. Erents, Errors in measuring electron temperatures using a single langmuir probe in a magnetic field, Plasma Phys. Control. Fus. 29 (3) (1987) 297.

[34] M.J. Martin, J. Bonde, W. Gekelman, P. Pribyl, A resistively heated CeB_6 emissive probe, Rev. Sci. Instrum. 86 (5) (2015) 053507. http://dx.doi.org/10.1063/1.4921838.

[35] J.C. Hosea, R.J. Perkins, M.A. Jaworski, G.J. Kramer, J.-W. Ahn, R.E. Bell, N. Bertelli, S. Gerhardt, T.K. Gray, B.P. LeBlanc, R. Maingi, C.K. Phillips, L. Roquemore, P.M. Ryan, S. Sabbagh, G. Taylor, K. Tritz, J.R. Wilson, S. Zweben, Predictions of V_{RF} on a Langmuir probe under the RF heating spiral on the divertor floor on NSTX-U, in: 41st European Physical Society Conference on Plasma Physics, 2014.

[36] F. Perkins, Radiofrequency sheaths and impurity generation by ICRF antennas, Nucl. Fus. 29 (4) (1989) 583.